ADVANCED FUNCTIONAL MATERIALS
www.afm-journal.de

Enhanced Variable Stiffness and Variable Stretchability Enabled by Phase-Changing Particulate Additives

*Trevor L. Buckner, Michelle C. Yuen, Sang Yup Kim, and Rebecca Kramer-Bottiglio**

A novel phase-changing particulate that amplifies a composite's modulus change in response to thermal stimulus is introduced. This particulate additive consists of a low melting point alloy (Field's metal; FM) formed into microparticles using a facile fabrication method, which enables its incorporation into polymer matrices using simple composite manufacturing processes. The effect of the solid–liquid phase change of the FM particles is demonstrated in two host materials: a thermally responsive epoxy and a silicone elastomer. In the epoxy matrix, this thermal response manifests as an amplified change in flexural modulus when heated, which is highly desirable for stiffness-changing move-and-hold applications. In the silicone matrix, the stretchability can be switched depending on the phase of the FM particles. This phenomenon allows the silicone to stretch and hold a strained configuration, and gives rise to mechanically programmable anisotropy through reshaping of the FM inclusions. FM particles present many opportunities where on-demand tunable modulus is required, and is particularly relevant to soft robotics. Because the melting temperature of FM is near room temperature, triggering the phase change requires low power consumption. The utility of FM particle-containing composites as variable stiffness and variable stretchability elements for soft robotic applications is demonstrated.

1. Introduction

Mechanical structures that demonstrate a change in stiffness are sought after in a variety of applications.[1] Such a structure might simply change its mechanical impedance to influence system dynamics, as seen in the human body when co-contraction of antagonistic muscles can increase a joint's resistance to motion.[2] More frequently in the field of soft robotics, the use-case of variable-stiffness involves "move-and-hold" operations for which a variable-stiffness structure holds a particular orientation in space or rigidly supports a load, and later becomes deformable on demand to allow shape change or repositioning, as often used in medical endoscope design.[3] Both use-cases of variable-stiffness can be made possible through a variety of methods, including the use of opposing actuators to "lock" a joint in a specific position,[4,5] granular and layer jamming to hold an appendage in shape (often by applying vacuum),[6–9] inflating a bladder to stiffen a joint,[10,11] and manipulating magnetorheological fluid that stiffens in the presence of a magnetic field.[12–15]

Thermally responsive materials that soften with exposure to heat can also be used as the basis of a variable-stiffness structure.[16–20] After softening, the material can be plastically deformed into a new configuration which will be held passively (i.e., without external forces) when cooled and stiffened. An effective thermally responsive variable-stiffness material will exhibit a large change in stiffness over a working temperature range so as to minimize energy expenditure, transition time, and thermal damage to other system components. Thermally induced material softening occurs primarily under two phenomena: melting and glass transition. Melting a material naturally results in a very large change in stiffness as the material changes from a solid to a liquid, but necessitates a containing medium to prevent leakage.[21] Continuous, encapsulated blocks or networks of melting polymers,[22] waxes,[23] and metals[24–26] have all been used in variable-stiffness systems, reaching stiffness change ratios of 100–9000×, depending on the encapsulating material and method. However, melting can also result in discontinuous material segments as it flows apart, requiring an external force to rejoin them.[27] In contrast, materials undergoing a glass transition remain continuous, but experience a comparatively limited stiffness change, generally 5–100×.[16–19] Upon heating through the glass transition temperature (T_g), polymer chains increase in energy, becoming more mobile, and will thus readily slide past one another when subjected to force, resulting in a rubber-like behavior, while remaining solid.

In pursuing the desired properties of a stiffness-changing material, one might turn to composite material design. A composite material benefits from the combined properties of two or more component materials. The choice of components determines the behavior of the composite, and the wide variety of

T. L. Buckner, M. C. Yuen, Dr. S. Y. Kim, Prof. R. Kramer-Bottiglio
School of Engineering and Applied Science
Yale University
New Haven, CT 06520, USA
E-mail: rebecca.kramer@yale.edu
Dr. M. C. Yuen
School of Mechanical Engineering
Purdue University
West Lafayette, IN 47907, USA
The ORCID identification number(s) for the author(s) of this article can be found under https://doi.org/10.1002/adfm.201903368.

DOI: 10.1002/adfm.201903368

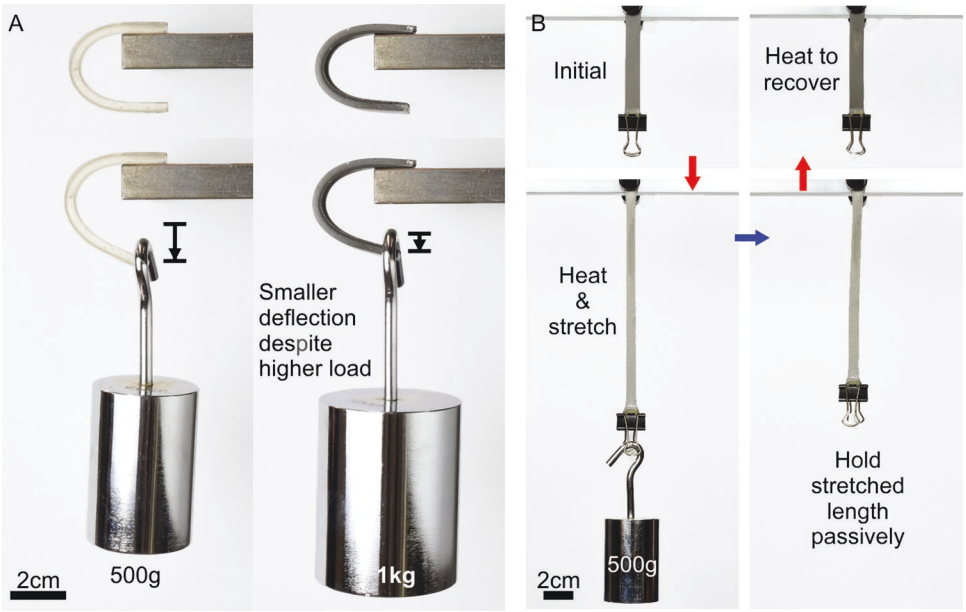

Figure 1. Field's metal/polymer composites. Field's metal is made into particles which can be mixed into polymers for variable modulus materials. A) Mixing FM particles into epoxy (right column) yields a material that exhibits an extended range of stiffness (as compared to neat epoxy, left column) when heated. At elevated temperatures, both specimens are able to be deformed to similar curvatures (top). Yet, at ambient temperatures, the FM/epoxy composite is stiffer than the neat epoxy and thus deflects less than the neat epoxy specimen (bottom). B) Mixing FM particles into silicone yields a "variable stretchability" material that is able to hold a deformed (stretched or compressed) state. Sequence starts in top left panel; the red arrows indicate heating phases; the blue arrow indicates a cooling phase.

matrix and filler materials available allow for tuning of specific material properties. Briefly, a filler additive might be chosen to increase mechanical strength, raise the elastic modulus, enhance thermal conductivity, or simply reduce product cost by using an inexpensive extender filler.[28–30] A filler material might also add a new property to an inert host material, such as endowing rubbers with electrical conductivity[31,32] or thermal conductivity,[33] or adding self-healing functionality to a polymer.[34] However, while composite filler materials can be specially chosen to alter a wide range of material properties, the ability to tune the range of stiffness change that a material experiences when subjected to heat is not a typical application of conventional fillers.

In this paper, we showcase a particulate additive which constitutes a new class of composite filler that is designed to undergo a repeatable, solid–liquid phase change during operation. To achieve this behavior, we selected microscale Field's metal (FM) particles as the additive material. Field's metal is a eutectic, fusible alloy of bismuth, indium, and tin with the following percentages by weight: 32.5% Bi, 51% In, 16.5% Sn. Field's metal melts at ≈62.5 °C, and can thus be melted easily in hot water. With a flexural modulus of ≈10 GPa (Figure S1, Supporting Information), FM is capable of a drastic, rapid change in stiffness at fairly low temperatures via the solid–liquid transition. We suspect that this class of phase-changing additive could be expanded in the future to include other similar materials such as other fusible metallic alloys (Cerrolow 117, Wood's metal) or possibly waxes and other polymers.[22–26,35]

Given the ease of rapid phase change, Field's metal particles act as a unique composite additive that substantially expand the range of modulus change of the composite material, although this behavior manifests differently depending on the matrix material. To demonstrate this effect, we present a series of composites that make use of microscale FM particles and explore their influence on material behavior, namely the change in stiffness by applying heat (**Figure 1**). We demonstrate how mixing FM particles in an epoxy matrix creates a material that exhibits variable stiffness behavior, as it transitions from a rigid to a compliant state through both the glass transition of the polymeric matrix and the melting of FM particles. We then demonstrate how the use of a stretchable silicone as the matrix yields a composite that is stretchable at room temperature, yet becomes much more stretchable when the FM particles are melted, a behavior that we will refer to as variable stretchability. FM is also highly electrically conductive, which allows it to be used as an electronic pathway or even as a solder.[36] We briefly characterize this property and its synergy with the variable-stiffness feature.

2. Results

The FM particles were fabricated by vigorously disrupting liquid-phase bulk Field's metal in hot water. A homogenizer was used to shear the bulk metal into smaller particles while simultaneously, an overhead mixer created a larger vortex to ensure all contents passed through the homogenizer. This method is similar to previously presented work for creating microparticles of low-melting-point materials[35,37] but allows processing of much larger volumes of material (60 g FM per batch vs 1.1 g[37]). The resulting particles were approximately spherical in shape and ranged in size from 10 to 800 µm in

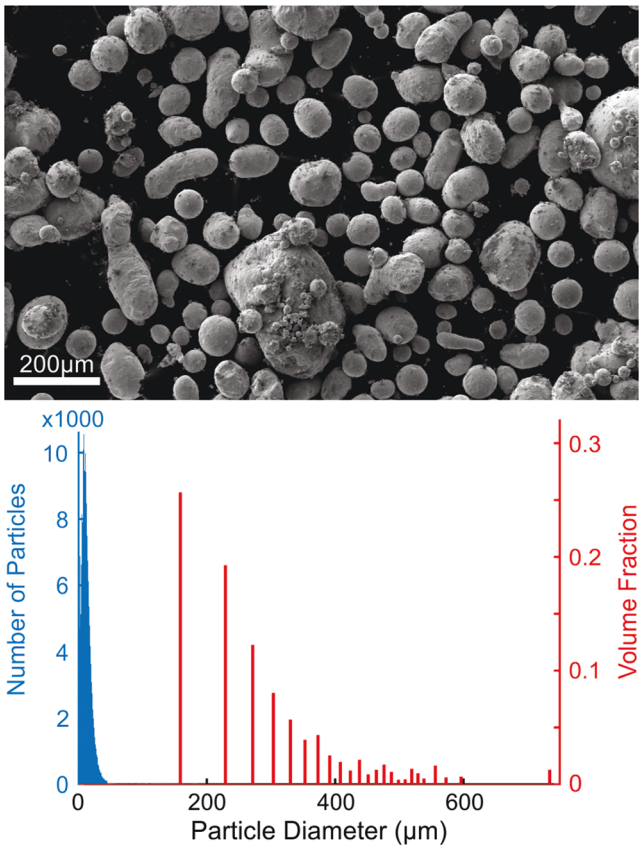

Figure 2. Morphological characteristics of field's metal particles. (Top) SEM image of Field's metal particles. (Bottom) Number and volume fraction distribution of Field's metal particles.

diameter (**Figure 2**; Figure S2, Supporting Information). Due to the high degree of nonuniformity in particle morphology in larger particles, only particles with diameter less than 355 μm were used in composite manufacture. The particle sizes had an approximately lognormal distribution with most (≈90%) particles by count being smaller than 100 μm in diameter. However, the volume of these smaller particles was negligible; larger diameter particles (>100 μm) comprised ≈96% of the total volume.

We mixed the FM particles at a range of volume fractions into two matrix materials to create an epoxy-based composite (FMEpoxy) and a silicone elastomer-based composite (FMSi) (Figure 1A,B, respectively). In order to gauge the modulus change offered by the FM particles, we characterized the effect of FM volume fraction on the stiffness of the composite over a temperature sweep using a dynamic mechanical analyzer (DMA).

2.1. Epoxy-Based Composite (FMEpoxy)

The epoxy we selected is a thermoset polymer that transitions from a stiff glassy state to a flexible rubbery state at $T_g \approx 35$ °C, making it useful for applications that require on-demand changes in stiffness. By adding increasing amounts of FM particles, the variable stiffness nature of the composite material is amplified further. As the composite material is heated, two distinct transitions are apparent: the glass transition of the epoxy, followed by the melting of the Field's metal inclusions (**Figure 3**A; Figures S3 and S4, Supporting Information). At high particle-loading (55 vol%), the stiffness of the epoxy in its glassy state ($T < T_g$) is amplified more than two-fold, relative to the neat (unmodified) epoxy (Figure 3B,D). While the composite is in the rubbery state but prior to melting of the Field's metal ($T_g < T < T_m$), increased Field's metal loading yields a higher stiffness. After melting ($T > T_m$), the stiffness of the composite is consistently low across all loading percentages, dropping slightly lower with larger volumes of the melted liquid metal. This result shows that incorporation of Field's metal simultaneously increases the rigid (cold) stiffness of the composite and reduces the lower (hot) stiffness bound when melted, thereby extending the total range of stiffness traversed by the composite material through a temperature sweep. This represents a stark increase in the rigid-to-soft modulus ratio from ≈400× to over ≈1500× (Figure 3C,D), and we compare this performance to the representative values of prominent examples of different types of variable stiffness mechanisms (**Figure 4**). Our results are in agreement with the theoretical results expected from the Halpin–Tsai composite model,[38] except at very high additive loading percentages, where the manufacturing process becomes inconsistent, as detailed further in Figure S5 (Supporting Information).

Often, it is desirable to Joule heat thermally responsive variable-stiffness materials via direct application of electrical current. This can be accomplished by making the material electrically conductive through the introduction of conductive particles, such as graphite,[39] carbon black,[40] or solid metal powder.[31] However, these additives also have the side effect of increasing both the upper and lower stiffness bounds of the composite (Figure 3E). Alternatively, conductive liquid metal can be used,[18] although this has the opposite effect of limiting the upper stiffness bound due to the presence of small pockets of liquid throughout the composite.

To overcome the tradeoff between increased electrical conductivity and a narrowed modulus window, we investigated as a secondary characteristic the effect of the FM additive on electrical conductivity of the epoxy composite (**Figure 5**). On its own, Field's metal is highly conductive, with a resistivity of $5.2 \times 10^{-7}\,\Omega$ m, or about 31 × that of copper.[41] However, until a certain volume fraction of conductive filler has been added, known as the percolation threshold, no bulk conductivity will be observed as the chances of individual particles coming in contact to form a continuous circuit are rare. The size and geometry of the particles greatly influence what this threshold might be. Spherical particles contribute to a very high percolation threshold, since all of the particulate mass is concentrated into isolated spheres of low aspect ratio. For this reason, even at up to 60% by volume, the FMEpoxy composite was not conductive. However, upon adding small amounts of carbon black (CB), which is also conductive and has a high surface area and branching, amorphous geometry, the small particles of Field's metal can be linked together, resulting in a conductive composite material that can be softened via Joule heating. By fixing the amount of carbon black at 3 vol% and gradually increasing the concentration of Field's metal, we observed

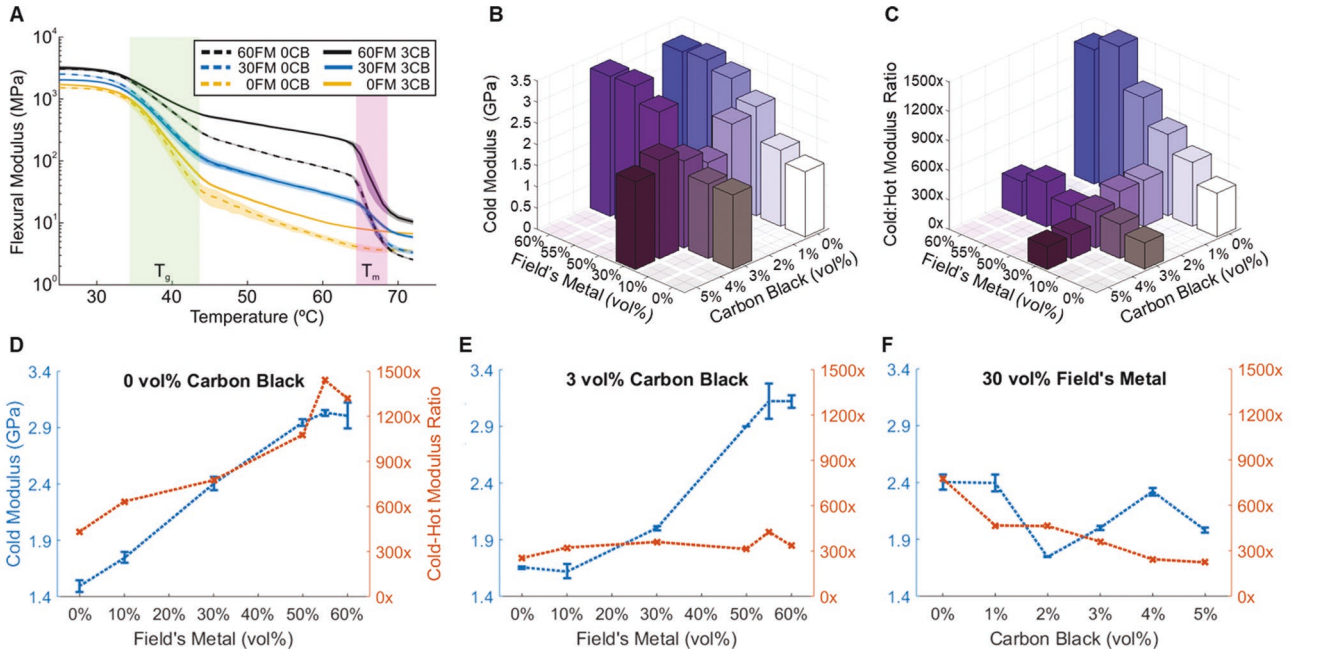

Figure 3. Stiffness measurements of Field's metal/epoxy composite material (FMEpoxy). A) Flexural modulus of the epoxy-based composites as a temperature sweep is applied by the DMA, passing through the epoxy glass transition (T_g) and Field's metal melting point (T_m). Composites contain varying volume percentages of Field's metal and carbon black. B) Flexural modulus of the epoxy-based composites at 23 °C (i.e., initial/cold stiffness) as a function of FM and CB volume fraction. C) Hot (72 °C) – cold (23 °C) flexural modulus ratio of the epoxy-based composites as a function of FM and CB volume fraction. D–F) The data from (B) and (C) reproduced as 2D scatterplots. D) As larger volumes of Field's metal are added to the composite, both the cold stiffness and ratio of stiffness change increase. E) With the inclusion of some amount of carbon black, increasing volumes of Field's metal continue to raise the cold stiffness. However, the stiffness ratio does not increase as dramatically due to the stiffening effect of carbon black even when heated. F) Further increasing the volume of carbon black does not seem to improve stiffness-change properties in any way. The plots show the mean response across three specimens of each composition; error bars indicate one standard deviation. Full datasets can be found in the Supporting Information.

that the conductivity does continue to rise, showing that FM particles do contribute to increased electrical conductivity of a composite (Figure 5B). To compare, we also held the volume of Field's metal constant at 30 vol% and adjusted the percentage of carbon black (Figure 5C). As expected, an increase in carbon black also leads to an increased electrical conductivity.

We note that for both FM and carbon black additives, the addition of large amounts of filler (above 50 vol% FM, or above 2 vol% CB) gives rise to manufacturing difficulties that result in defects (Figure 3F). In those cases, the composite slurry becomes thick and paste-like, resulting in trapped air pockets and an inability for the mixture to flow smoothly into its mold. We hypothesize that the resulting voids are the reason for the unexpected deviations from predicted behavior at high loading percentages. Carbon black in particular appears to contribute to significantly higher porosity in specimens even at very low volume percentages, resulting in a cold state that is softer than expected, while still raising the stiffness of the warm state due to the stiffening effect of CB (Figure S4, Supporting Information). These effects partially counteract the stiffness-change enhancements granted by the FM particles; further research may reveal a more compatible conductive material that synergistically lowers the percolation threshold for FM particles with fewer negative effects. Additionally, FM particles with a higher aspect ratio could have more favorable effects on conductivity.

To simulate the deformations expected during use of these materials, we compared the deflection of FMEpoxy cantilever samples (neat epoxy, 30%FM 0%CB, 30%FM 3%CB) (**Figure 6**A; Figures S6 and S7, Supporting Information) of size 80 mm × 10 mm × 3.7 mm. At room temperature, the neat epoxy clearly deflected the most under a 200 g load, followed by the 30FM 3CB, and lastly the 30FM 0CB sample when subjected to the same loading conditions. Though the 30FM 3CB is expected to be stiffer than the 30FM 0CB due to the stiffening effect of carbon black particles, the above-mentioned manufacturing difficulties with CB resulted in a more flexible composite due to a higher concentration of voids. In the soft state, all samples collapse under only 50 g, exhibiting nearly the same deflection. This demonstration shows that the addition of Field's metal particles clearly enhances the stiffness when cold without adversely increasing the stiffness in the heated state.

An application of the FMEpoxy in a soft robotic actuator is shown in Figure 6B and in Movie S1 (Supporting Information). Silicone-based Pneunet actuators are designed to bend when inflated; removing the inflation pressure allows the stretched silicone to relax back into a flat configuration. By affixing a thin layer of FMEpoxy to the strain-limiting layer, the actuator can perform move-and-hold operations. Softening the FMEpoxy via Joule heating (or otherwise) allows the actuator to bend when inflated. After cooling, the new plastically deformed configuration will be maintained even after the actuator is deflated. Furthermore, the FMEpoxy in the stiff state resists bending when the actuator is inflated.

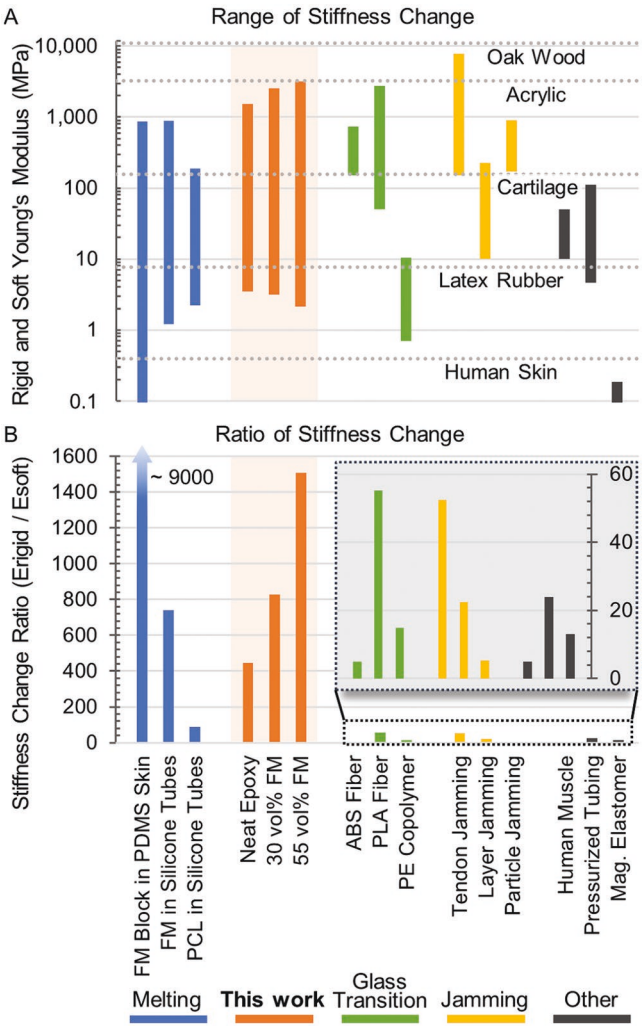

Figure 4. Comparison of stiffness-change performance to representative results in the literature. The FMEpoxy composite shows high stiffness-change performance when compared to other variable-stiffness methods. The range of stiffness change is orders of magnitude above most techniques, second only to methods that involve melting continuous blocks of metal. Because of this, the FMEpoxy can become softer than natural latex rubber, which can be deformed even by low-force actuators. On the other hand, the stiffened composite is similar to rigid acrylic, which can act as a lightweight, yet sturdy structural element able to withstand a great deal of force. The variable stiffness methods in this figure, in order, include melting techniques: solid blocks of FM in a polydimethylsiloxane (PDMS) skin,[24] FM in silicone tubing,[27] polycaprolactone (PCL) polymer in silicone tubing;[22] this work: neat SMP epoxy, epoxy with 30 vol% FM loading, and epoxy with 55 vol% FM loading; glass transition techniques: Acrylonitrile butadiene styrene (ABS) polymer,[17] polylactic acid (PLA) polymer,[45] polyethylene (PE) copolymer;[18] jamming techniques: tendon jamming,[46] layer jamming,[47] particle jamming;[48] and some other types: flexing of natural skeletal muscle in a living human,[40] high internal pressure in a tube,[49] and magnetorheological elastomers.[50]

2.2. Silicone-Based Composite (FMSi)

Because silicone elastomers have a T_g far below our working temperature range, the FMSi exhibited a single transition—the melting of the FM particles (**Figure 7**A; Figure S8, Supporting Information). Predictably, the addition of FM particles progressively stiffens the composite while the particles remain as solid-phase. However, in contrast to the FMEpoxy, the liquid-phase FM inclusions also contributed to a minor increase in the composites' stiffness, relative to neat silicone. We hypothesize that this may be due to a combination of two factors: 1) We suspect that the majority of this stiffness occurs due to regions of phase-separated metal that fail to melt at or near the eutectic point.[37] Formation of a thin solid oxide shell on the droplet surface and oxide fragments that remain solid at elevated temperatures may also have played a significant role in this stiffening behavior.[36] 2) To a lesser extent, small liquid droplets $\left(D \leq \frac{\gamma}{E}\right)$ with sufficient surface tension ($\gamma \approx 387.17$ mN m^{-1}, Figure S9, Supporting Information) in sufficiently soft solids (Young's modulus, $E \approx$ 100–200 kPa) are known to behave more rigidly than predicted by the rule of mixtures and the Halpin–Tsai theory regarding stiffness of composite materials (Figure S5, Supporting Information).[33,38,42] At these small length scales, the surface tension of the liquid-phase FM inclusions resists the imposed deformation of the host matrix, effectively increasing the stiffness of the composite. However, from the particle distribution found previously, particles smaller than this characteristic length scale ($D \leqslant 2\,\mu$m) comprise only ≈7% of all particles (by count), which contributes only marginally to this phenomenon.

In addition to the stiffness measurements of the as-prepared samples over a temperature sweep, we tested samples that were subjected to two modes of deformation, compression and tension, each along two axes (Figure 7B, Supporting Information). The stiffnesses of the samples were measured at 25 °C prior to any deformation, while in the deformed state, and after recovery to the original shape. To deform the samples, we heated the FMSi in hot water to melt the FM, deformed the sample (20% compression strain or 50% extension strain), and then quenched the FMSi in cold water while holding it in its deformed state until the Field's metal resolidified. To evaluate if any permanent damage occurred as a result of deformation, samples were returned to their original shape by melting the FM in hot water once again and letting the silicone matrix pull itself back into its original shape. We found that the deformation processes had minimal effect on the stiffness of the composite; the stretched samples exhibited a slightly lower stiffness after recovering its original shape.

The samples showed clear changes in stiffness while in the deformed, cooled state. Compressing the sample narrower (presumably forming vertical FM "pancakes") and stretching the sample longer (forming FM "needles" along the length, see Movie S2 in the Supporting Information) resulted in a significant increase in stiffness. These vertical FM "pancakes" and the lengthwise "needles" would be aligned with the compression and tension stresses applied by the DMA during the bending tests and thus would be able to take more of the load, resulting in a higher stiffness. Compressing the sample flatter (forming horizontal FM "pancakes") also resulted in stiffening due to FM inclusions taking on a similar role to that of the lengthwise "needles," but to a lesser extent. Lastly, stretching the sample wider (forming FM "needles" parallel to the neutral axis of the cross-section) reduced the vertical height of the FM inclusions and resulted in a slight decrease in stiffness. These results indicate

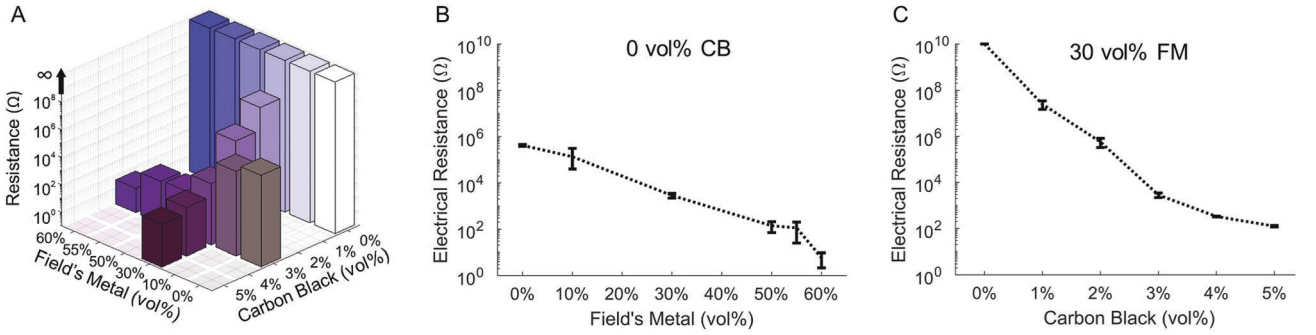

Figure 5. Electrical conductivity measurements of Field's metal/epoxy composite material (FMEpoxy). A) Electrical conductivity of the epoxy-based composites as volume percentages of Field's metal and carbon black are varied. On its own, any amount of Field's metal does not result in a conductive composite. B,C) The data from A) reproduced as 2D scatterplots. B) With the inclusion of some amount of carbon black, increasing volumes of Field's metal continue to lower the electrical resistivity of the composite. C) Further increasing the volume of carbon black continues to lower the resistivity of the composite. The plots show the mean response across three specimens of each composition; error bars indicate one standard deviation.

that cooling the FMSi composite in a deformed state creates a material with anisotropic mechanical properties. Moreover, this deformation is fully reversible and the original as-cast shape of the FMSi can be fully recovered by applying heat to allow the FM inclusions to return to their roughly spherical shape.

To demonstrate the stretch-and-hold capability of the silicone-based composite, we first heated and stretched a specimen by hanging a weight (Figure 1B; Figure S10, Supporting Information). We then let the FM particles solidify and removed the weight, showing that the sample stayed stretched, holding 87% of its elongation. Finally, we reheated the sample, allowing it to recover its original shape. Additionally, we found that the spring stiffness of the silicone-based composite decreased by 5.2× when the FM particles were melted, as compared to the stiffness when the FM particles were solid in an undeformed state (Figure S10, Supporting Information). The results shown here closely parallel those shown by van Meerbeek et al. wherein an open-cell silicone foam was infused with Field's metal to perform similar stretch-and-hold operations.[21] However, our FMSi composite remains soft, stretchable, and flexible throughout its operating temperature range, rather than switching between a stiff, rigid state (i.e., a porous metal element) and a soft, compliant state (i.e., a porous silicone foam). The persistent compliance of the FMSi is especially advantageous for integration into soft robotic applications, as demonstrated below. Additionally, the particulate composite nature of the FMSi and its ability to hold deformed shapes via deformation of FM particles is similar to the work presented by Chang et al., however here, we focus on leveraging the repeatable phase-change transition of the FM particles.[43]

We used the FMSi to create an on-demand pop-up tactile display, a bidirectional pneumatic gripper, and a multitrajectory pneumatic actuator (**Figure 8**). In the pop-up tactile display, flat bladders were first patterned into a silicone film, and a film of the FMSi composite was bonded to the top (Figure 8A; Movie S3, Supporting Information). The FMSi was heated and the

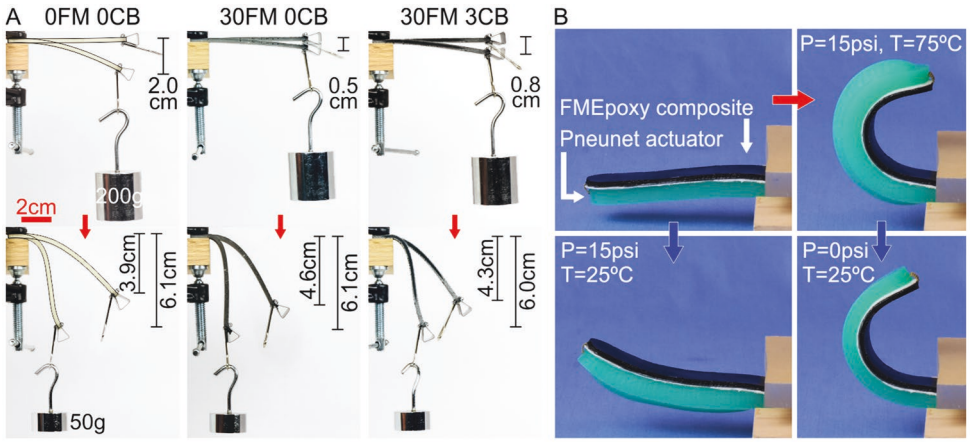

Figure 6. Applications of Field's metal/epoxy composite material (FMEpoxy). A) Demonstration of the change in stiffness when the epoxy-based materials are heated from 20 °C (top row) to 70 °C (bottom row). The composites (middle and right columns) show a stiffer (less deflected) cold state compared to the neat epoxy (left column; outlined for clarity). After heating, the self-weight of the composites causes them to droop more than the neat epoxy. When loaded, it is apparent that the composites are as soft as the neat epoxy. B) Application of the FMEpoxy material in a pneumatically actuated bending actuator for a move-and-hold operation. Red arrows indicate heating; blue arrows indicate cooling phases. When the FMEpoxy is hot, the bending actuator is able to inflate and curl (top right vs bottom left). After the FMEpoxy cools while in the bent state, the actuator holds its bent configuration even with the inflation pressure removed (bottom right).

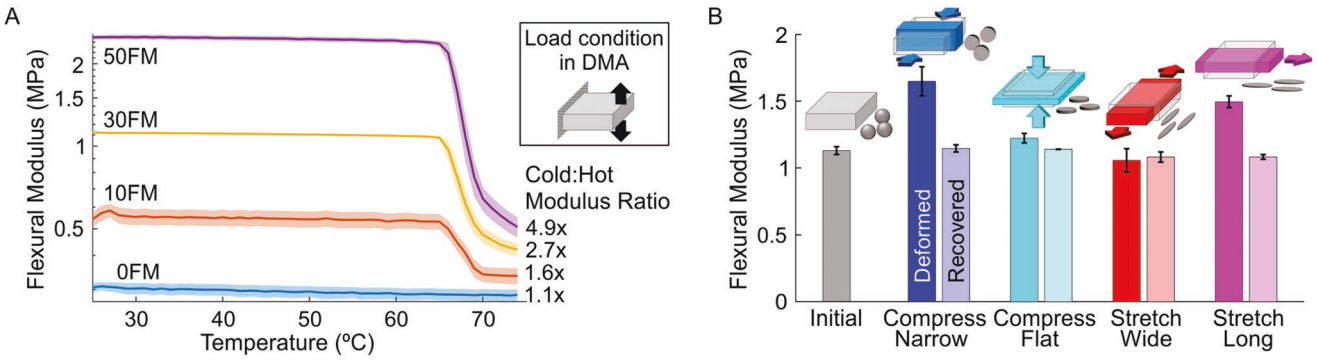

Figure 7. Stiffness measurements of Field's metal/silicone composite material (FMSi). A) Flexural modulus (mean ± standard deviation) of the silicone-based composite as measured in the DMA as a temperature ramp is applied. The plots show the mean response across three specimens of each composition; the error clouds indicate one standard deviation. Full datasets can be found in the Supporting Information. The same single-cantilever loading condition was used across all DMA characterization experiments. B) Cold stiffnesses of the silicone-based composite prior to deformation (initial; gray bar), after deforming and cooling in place (darker colored bar), and after heating to recover its original shape (lighter colored bar). The schematics show the mode and direction of deformation applied and the resulting morphology ('pancake', 'needle') of an initially spherical Field's metal particle. The direction of deformation is drawn with respect to the same coordinate frame as the load condition schematic in (A).

bladders were inflated, stretching the FMSi. While maintaining the inflation, the FMSi film was allowed to cool to capture the pop-up bubble shape. After the air was removed, the FMSi film retained the inflated shape, creating a potential interactive display on demand. Upon heating the film again, the display returned to a fully flat state.

For the second application of the FMSi composite, we fabricated a Pneunet powered soft gripper[44] out of a soft silicone material with the FMSi as a stiffer layer on the bottom (Figure 8B; Movie S4, Supporting Information). Upon inflation, the soft silicone stretched more than the stiffer FMSi, causing the gripper to close downward. While maintaining the inflation, the gripper was placed in hot water, melting the Field's metal particles. This resulted in the bottom FMSi layer becoming even softer than the silicone material, and for the gripper to flip and close in the other direction with the FMSi on the outer stretched layer. The gripper was then submerged in cold water to freeze the FM particles in the flipped gripper configuration. After removing the inflation, the gripper stayed in the closed configuration because the FMSi was cooled in a stretched state. Upon reimmersion in hot water, the FM melted, allowing the gripper to reset itself into a flat configuration.

Lastly, we coated a flat pneumatic bladder with FMSi on either side (Figure 8C). We selectively heated up sides or regions of the FMSi and then inflated the bladder. When one FMSi side of the bladder was heated, the actuator displayed a curved configuration because heated regions were able to stretch more than the cool regions. When both sides were heated, the actuator simply elongated. Finally, when only a portion of the FMSi was heated, the actuator inflated into a partially curved state. These simple demonstrations illustrate the potential of using FMSi as a method to control the motion of soft, inflated structures using targeted heating.

3. Discussion and Conclusions

Field's metal is a promising phase-changing material for tuning the modulus of structures because its melting temperature is so close to room temperature. However, processing and patterning bulk Field's metal blocks or networks can be difficult compared to processing of polymer-based composites. The manufacturing method to create Field's metal particles at unprecedented volumes thus extends the potential impact and utilization of Field's metal because now it can be used as a functional inclusion in a composite material system. We are motivated by the field of soft robotics and thus are particularly interested in variable stiffness materials. By mixing the Field's metal particles into specific polymers, namely epoxy and silicone, we can leverage each material's functional properties and extract even more use from the composite than from the constituent materials separately.

Field's metal particles as inclusions in polymer-based composites yield enhanced stiffness change when coupled with glass-transition polymers and endow elastomers with variable stretchability properties. Here, we showed that Field's metal particles in an epoxy matrix increased the "cold" stiffness of the material by up to 3×, and unlike permanently solid inclusions, did not raise the "hot" stiffness, but instead lowered it slightly. The addition of carbon black particles allowed the electrical conductivity of the FM to contribute to the overall electrical conductivity of the composite, allowing Joule heating to be used to soften the epoxy and melt the Field's metal. Silicone elastomers with embedded Field's metal particles exhibit increased stiffness compared to neat silicone both when the Field's metal is solidified and melted. We demonstrated that the particles can be leveraged for variable stretchability and for performing stretch-and-hold operations. Furthermore, the altered morphology of the Field's metal particles during "stretch-and-hold" operations results in anisotropic stiffness in the material.

4. Experimental Methods

Field's Metal Particle Fabrication: Field's metal particles were created in by melting the metal in warm water and agitating vigorously. A block of Field's metal (Roto144F, RotoMetals) is weighed out to 60 g. 150 mL of deionized water was added to a 500 mL beaker and the Field's metal was placed inside. A silicone oil bath was heated on

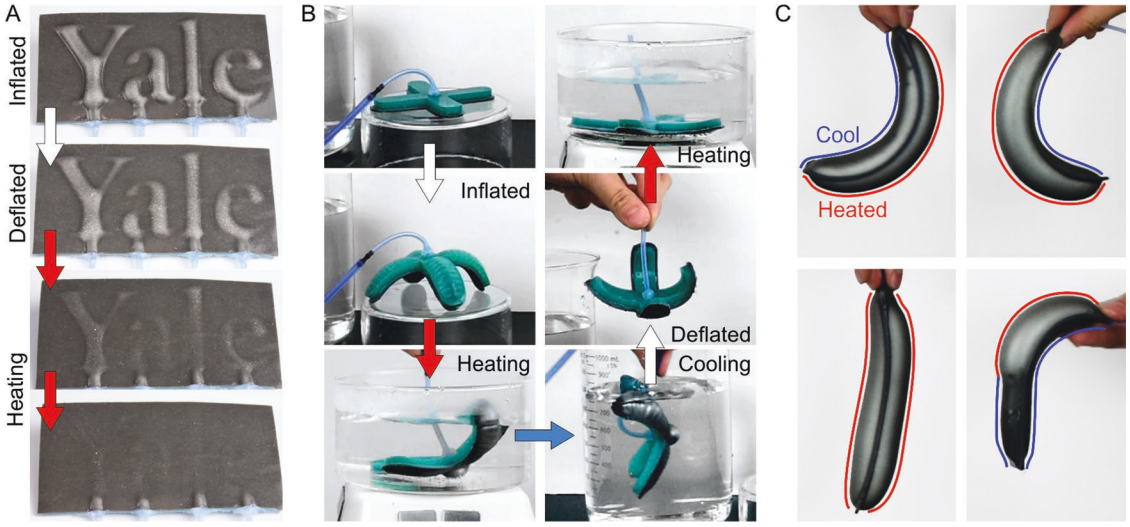

Figure 8. Applications of Field's metal/silicone composite material (FMSi). A) FMSi film (30 vol% FM) used to create pop-up displays and buttons in a silicone membrane patterned with flat, inflatable pockets. From top to bottom, the bladders are: heated and inflated, resolidified and deflated, heated, fully recovered. B) FMSi film (30 vol% FM) integrated into a pneumatically actuated gripper for bidirectional grasping. Switching between the solid and liquid FM particles causes the FMSi layer to alter between being stiffer than the silicone body (shown in green) and being more stretchable, which enables control of the direction of the grasping motion. C) A flat, pneumatic bladder was coated on both sides with a layer of FMSi. Heating up specific sides or regions of the FMSi allows for control of the bladder trajectory when inflated.

a hot plate with a magnetic stirring rod up to 90 °C, and the 500 mL beaker was supported inside the silicone oil bath such that the water level was below the surface of the oil. The water was allowed to warm for ≈15 min until it settled at ≈70 °C and the metal was fully melted. At this stage, a mechanical homogenizer (VDI25, VWR) with a 20 mm diameter attachment and a vortex generator (RW16, IKA-werke) with a 42 mm diameter turbine attachment were placed into the water on opposite sides of the beaker. The beaker was tilted slightly such that the heavy metal will flow downward toward the homogenizer rather than gathering at the edges of the beaker. At this point, the homogenizer was turned on to a speed of 24 000 rpm and manually swept through the mixture for several seconds so as to initially break up the mass of metal which is held together by surface tension, dispersing it into the water. The homogenizer was turned off and then fixed in place. With both instruments in position, the homogenizer was again turned on to a speed of 24 000 rpm to further break up the melted particles, and the vortex generator was turned on to a speed of 1200 rpm, which keeps the metal in motion and prevents it from settling and agglomerating. This agitation was applied for 10 min.

Next, the beaker was quickly raised out of the hot silicone oil bath to cool. The vortex generator remained on to keep particles in motion until they had cooled solid, but the homogenizer was turned off so as not to shatter the solidified particles, creating unpredictable particle geometries and sizes. The mixture was allowed to cool for ≈15 min until its temperature was well below the freezing point of Field's metal (≤50 °C), at which point the vortex generator was turned off, and the mixture was allowed to settle. After several hours, the majority of the particles settled to the bottom of the beaker, and the supernatant was extracted via syringe (rather than pouring) so as not to disturb the small particles. The remaining particle sediment was then stirred and "fluffed" to minimize any cementing during the drying process. The particles were dried in a vacuum oven at 60 °C to remove as much of the remaining moisture as possible. The resulting dry material may clump together like sandstone and need to be shaken apart. The resulting material had a fine, sand-like appearance.

Carbon Black Preparation: Carbon black pellets (PRINTEX XE2-B, Orion Engineered Carbons) were broken apart in a commercial blender (Hamilton Beach) by pulsing at maximum speed for 5 min. The resulting particles are ≈5 µm in diameter as measured in a scanning electron microscope.

Epoxy Composite Fabrication: The epoxy composite is a polydisperse mixture of both Field's metal and carbon black particles suspended in a two-part polymer epoxy. First, the epoxy was created by combining an epoxy curing agent, Jeffamine D400 (Huntsman International, LLC), with a standard epoxy resin, EPON 828 (Momentive Performance Materials Inc.) at a ratio of 4:10 by weight. This ratio is well below the stoichiometric ratio of 58:100, resulting in a softer material and a lower glass transition temperature. This mixing ratio was chosen to move the epoxy glass transition temperature below the melting temperature of Field's metal to clearly demonstrate them as two separate transitions. After stirring lightly by hand, the epoxy mixture was placed in a vacuum chamber for 15 min to reduce porosity by removing trapped air. At this stage, the desired amounts of Field's metal and carbon black particles were measured out by weight, then poured into a measured portion of epoxy and stirred by hand until thoroughly dispersed. The resulting composite was then poured or scooped into a mold as required depending on the thickness of the mixture. The composite was allowed to reach a gel state over 16 h at room temperature, which further reduces the presence of voids which may form by heating of air pockets in the material in the next step. Finally, the gelled composite was placed in an incubator at 60 °C for at least 12 h for final curing.

Silicone Composite Fabrication: The silicone composite is a polydisperse mixture of Field's metal particles suspended in a silicone matrix. The appropriate mass of Field's metal particles was measured out into a container. The two parts of the silicone (DragonSkin 10 Slow, Smooth-On) were then mixed together using a planetary mixer (Thinky ARE-310) and then measured out into the same container as the Field's metal particles. The two constituents were stirred together until the Field's metal particles were well dispersed in the silicone. The mixture was then poured into molds or cast into films. All samples were allowed to degas in ambient conditions, rather than under vacuum. The specimens were then cured for a minimum of 6 h prior to use.

DMA Testing: Stiffness change was measured using a dynamic mechanical analyzer (DMA Q800, TA Instruments). Composite specimen dimensions were determined such that the expected minimum and maximum stiffness measurements were both within the measurement range of the equipment. For epoxy samples, this was 30 mm × 12.5 mm × 5 mm. For silicone samples, this was 30 mm × 15 mm × 5 mm. Specimens were placed in a single-cantilever clamp. Assuming the two ends of the specimen are clamped and do

not rotate, the specimen flexural modulus E_f can be calculated from the measured force: $E_f = FL^3/12\delta I$, where L is the length of the beam, I is the area moment of inertia of its cross-section, and F is the force needed to deflect the beam a distance δ.

DMA Testing—Epoxy Composite Stiffness Measurement: The epoxy composite samples were applied a temperature sweep from 20 to 80 °C at a rate of 1 °C min^{-1}, around the phase transition zones from 30 to 40 °C (epoxy glass transition) and from 60 to 70 °C (metal melting), then at 5 °C min^{-1} everywhere else. Specimens were applied a sinusoidal force on the moving end of cantilever at a rate of 5 Hz, at a strain of 0.01%. Specimens were clamped at a torque of 6 in lbs.

DMA Testing—Silicone Composite Stiffness Measurement: The silicone composite samples were applied a temperature sweep from 20 to 80 °C at a rate of 1 °C min^{-1}, around the single phase transition zone from 60 to 70 °C (metal melting), then at 5 °C min^{-1} everywhere else. Specimens were applied a sinusoidal force on the moving end of cantilever at a rate of 5 Hz, at a strain of 3.75%. Specimens were clamped at a torque of 2 in lbs (0.226 N m). For the deformed samples, the specimens were compressed to 20% strain or stretched to 50% strain. Upon release of load, the specimens relaxed: CompressNarrow retained 13.3% compressive strain; CompressFlat retained 18.2% compressive strain; StretchWide retained 42.1% tensile strain; and StretchLong retained 44.4% tensile strain.

Supporting Information

Supporting Information is available from the Wiley Online Library or from the author.

Acknowledgements

T.L.B. and M.C.Y. contributed equally to this work. The authors would like to thank Jennifer C. Case and R. Adam Bilodeau for their helpful insights. The DMA instrument was supported under the auspices of the National Science Foundation by Harvard's Materials Research Science and Engineering Center (DMR-1420570). This work was supported by the US Air Force Office of Scientific Research (FA9550-16-1-0267) and the National Science Foundation (EFMA-1830870).

Conflict of Interest

The authors declare no conflict of interest.

Keywords

multifunctional materials, soft robotics, variable stiffness, variable stretchability

Received: April 27, 2019
Revised: July 1, 2019
Published online:

[1] M. Manti, V. Cacucciolo, M. Cianchetti, *IEEE Rob. Autom. Mag.* **2016**, *23*, 93.
[2] I. Hunter, S. Lafontaine, in *Technical Digest IEEE Solid-State Sensor and Actuator Workshop*, IEEE, Hilton Head Island, SC, USA, **1992**, pp. 178–185.
[3] L. Blanc, A. Delchambre, P. Lambert, *Actuators* **2017**, *6*, 23.
[4] M. T. Gillespie, C. M. Best, M. D. Killpack, in *2016 IEEE Int. Conf. on Robotics and Automation (ICRA)* (Ed: A. Okamura), Stockholm, Sweden **2016**, pp. 1095–1101.
[5] G. Tonietti, A. Bicchi, in *IEEE/RSJ Int. Conf. on Intelligent Robots and Systems*, Vol. *2*, Lausanne, Switzerland **2002**, pp. 1992–1997.
[6] E. Brown, N. Rodenberg, J. Amend, A. Mozeika, E. Steltz, M. R. Zakin, H. Lipson, H. M. Jaeger, *Proc. Natl. Acad. Sci. USA* **2010**, *107*, 18809.
[7] Y. Li, Y. Chen, Y. Yang, Y. Wei, *IEEE Trans. Robot.* **2017**, *33*, 446.
[8] Y. Kim, S. Cheng, S. Kim, K. Iagnemma, *IEEE Trans. Robot.* **2013**, *29*, 1031.
[9] J. Ou, L. Yao, D. Tauber, J. Steimle, R. Niiyama, H. Ishii, in *Proceedings of the 8th Int. Conf. on Tangible, Embedded and Embodied Interaction*, TEI '14, ACM, New York, NY, USA **2013**, pp. 65–72.
[10] B. Vanderborght, A. Albu-Schaeffer, A. Bicchi, E. Burdet, D. G. Caldwell, R. Carloni, M. Catalano, O. Eiberger, W. Friedl, G. Ganesh, M. Garabini, M. Grebenstein, G. Grioli, S. Haddadin, H. Hoppner, A. Jafari, M. Laffranchi, D. Lefeber, F. Petit, S. Stramigioli, N. Tsagarakis, M. Van Damme, R. Van Ham, L. C. Visser, S. Wolf, *Robot. Auton. Syst.* **2013**, *61*, 1601.
[11] D. G. Caldwell, G. A. Medrano-Cerda, M. Goodwin, *IEEE Control Syst. Mag.* **1995**, *15*, 40.
[12] J. D. Carlson, M. R. Jolly, *Mechatronics* **2000**, *10*, 555.
[13] C. Majidi, R. J. Wood, *Appl. Phys. Lett.* **2010**, *97*, 164104.
[14] G. Y. Zhou, Q. Wang, *Smart Mater. Struct.* **2006**, *15*, 59.
[15] P. Testa, R. W. Style, J. Cui, C. Donnelly, E. Borisova, P. M. Derlet, E. R. Dufresne, L. J. Heyderman, *Adv. Mater.* **2019**, *31*, 1900561.
[16] T. Chenal, J. Case, J. Paik, R. Kramer, in *2014 IEEE/RSJ Int. Conf. on Intelligent Robots and Systems (IROS 2014)* (Ed: W. Burgard), IEEE, Chicago, IL, USA **2014**, pp. 2827–2831.
[17] M. C. Yuen, R. A. Bilodeau, R. K. Kramer, *IEEE Rob. Autom. Lett.* **2016**, *1*, 708.
[18] S. Rich, S.-H. Jang, Y.-L. Park, C. Majidi, *Adv. Mater. Technol.* **2017**, *2*, 1700179.
[19] A. Balasubramanian, M. Standish, C. J. Bettinger, *Adv. Funct. Mater.* **2014**, *24*, 4860.
[20] L. Wang, Y. Yang, Y. Chen, C. Majidi, F. Iida, E. Askounis, Q. Pei, *Mater. Today* **2018**, *21*, 563.
[21] I. M. V. Meerbeek, B. C. M. Murray, J. W. Kim, S. S. Robinson, P. X. Zou, M. N. Silberstein, R. F. Shepherd, *Adv. Mater.* **2016**, *28*, 2801.
[22] M. A. McEvoy, N. Correll, *J. Compos. Mater.* **2015**, *49*, 1799.
[23] N. G. Cheng, A. Gopinath, L. Wang, K. Iagnemma, A. E. Hosoi, *Macromol. Mater. Eng.* **2014**, *299*, 1279.
[24] W. Shan, T. Lu, C. Majidi, *Smart Mater. Struct.* **2013**, *22*, 085005.
[25] W. Wang, H. Rodrigue, S.-H. Ahn, *Composites, Part B* **2015**, *78*, 507.
[26] S. Yoshida, Y. Morimoto, L. Zheng, H. Onoe, S. Takeuchi, *Soft Rob.* **2018**, *5*, 718.
[27] A. Tonazzini, S. Mintchev, B. Schubert, B. Mazzolai, J. Shintake, D. Floreano, *Adv. Mater.* **2016**, *28*, 10142.
[28] H. S. Katz, J. V. Mileski, *Handbook of Fillers for Plastics*, Elsevier, Amsterdam, Netherlands **1987**, https://onlinelibrary.wiley.com/doi/full/10.1002/adfm.201303905.
[29] R. C. R. Nunes, J. L. C. Fonseca, M. R. Pereira, *Polym. Test.* **2000**, *19*, 93.
[30] R. F. Gibson, *Compos. Struct.* **2010**, *92*, 2793.
[31] Y. P. Mamunya, V. V. Davydenko, P. Pissis, E. V. Lebedev, *Eur. Polym. J.* **2002**, *38*, 1887.
[32] M. Park, J. Park, U. Jeong, *Nano Today* **2014**, *9*, 244.
[33] M. D. Bartlett, N. Kazem, M. J. Powell-Palm, X. Huang, W. Sun, J. A. Malen, C. Majidi, *Proc. Natl. Acad. Sci. USA* **2017**, 201616377.
[34] S. R. White, N. R. Sottos, P. H. Geubelle, J. S. Moore, M. R. Kessler, S. R. Sriram, E. N. Brown, S. Viswanathan, *Nature* **2001**, *409*, 794.

[35] M. Baginska, B. J. Blaiszik, S. A. Odom, A. E. Esser-Kahn, M. M. Caruso, J. S. Moore, N. R. Sottos, S. R. White, in *Experimental Mechanics on Emerging Energy Systems and Materials*, Vol. *5* (Ed.: T. Proulx), Conf. Proc. of the Society for Experimental Mechanics Series, Springer, New York, **2011**, pp. 17–23.
[36] S. Çinar, I. D. Tevis, J. Chen, M. Thuo, *Sci. Rep.* **2016**, *6*, 21864.
[37] I. D. Tevis, L. B. Newcomb, M. Thuo, *Langmuir* **2014**, *30*, 14308.
[38] J. C. Halpin, S. W. Tsai, Technical Report AFML-TR-67-423, Air Force Materials Lab Wright-Patterson AFB, OH, **1969**.
[39] T. L. Buckner, E. L. White, M. C. Yuen, R. A. Bilodeau, R. K. Kramer, in *2017 IEEE/RSJ Int. Conf. on Intelligent Robots and Systems (IROS)*, **2017**, IEEE, pp. 3728–3733.
[40] W. Shan, S. Diller, A. Tutcuoglu, C. Majidi, *Smart Mater. Struct.* **2015**, *24*, 065001.
[41] Y. Han, J. Dong, *Adv. Mater. Technol.* **2018**, *3*, 1700268.
[42] R. W. Style, R. Boltyanskiy, B. Allen, K. E. Jensen, H. P. Foote, J. Wettlaufer, E. R. Dufresne, *Nat. Phys.* **2015**, *11*, 82.
[43] B. S. Chang, et al., *Mater. Horiz.* **2018**.
[44] F. Ilievski, A. D. Mazzeo, R. F. Shepherd, X. Chen, G. M. Whitesides, *Angew. Chem.* **2011**, *123*, 1930.
[45] S. Kamthai, R. Magaraphan, *AIP Conf. Proc.* **2015**, *1664*, 060006.
[46] T. M. Huh, Y.-J. Park, K.-J. Cho, *Int. J. Precis. Eng. Manuf.* **2012**, *13*, 1255.
[47] S. Kawamura, T. Yamamoto, D. Ishida, T. Ogata, Y. Nakayama, O. Tabata, S. Sugiyama, in *Proc. 2002 IEEE Int. Conf. on Robotics and Automation (Cat. No. 02CH37292)*, Vol. *1*, IEEE, Washington DC, USA **2002**, pp. 248–253.
[48] A. Jiang, G. Xynogalas, P. Dasgupta, K. Althoefer, T. Nanayakkara, in *2012 IEEE/RSJ Int. Conf. on Intelligent Robots and Systems*, IEEE, Vilamoura, Algarve, Portugal **2012**, pp. 2922–2927.
[49] Y. Shan, M. Philen, A. Lotfi, S. Li, C. E. Bakis, C. D. Rahn, K. Wang, *J. Intell. Mater. Syst. Struct.* **2009**, *20*, 443.
[50] Y. Li, J. Li, T. Tian, W. Li, *Smart Mater. Struct.* **2013**, *22*, 095020.